SLAC-PUB-2801
September 1981
(T/E)

# SPEAR RESULTS - 1981*

Daniel L. Scharre
Stanford Linear Accelerator Center
Stanford University, Stanford, CA 94305

ABSTRACT

New results from SPEAR on the inclusive photon spectrum at the $\psi'$ and on $J/\psi$ radiative transitions are presented. Evidence for an $\eta_c'$ candidate is observed in the $\psi'$ inclusive photon spectrum at a mass M = 3592 ± 5 MeV. A new resonance, the $\theta(1640)$ which is observed to decay into $\eta\eta$, has been seen in radiative transitions from the $J/\psi$. The spin-parity of the $\iota(1440)$, previously observed in $J/\psi$ radiative transitions and originally identified as the E(1420), has been determined to be $0^-$.

## I. INTRODUCTION

The number of new physics results which have come from the Crystal Ball[1] and Mark II[2] experiments at SPEAR during the past year is so great that it is impossible to do justice to all of the work in the short amount of time available for this talk. For this reason, I have chosen the two topics which I consider to be the newest and most exciting to present.

- Analysis of the $\psi'$ inclusive photon spectrum by the Crystal Ball. Of particular interest is evidence for an $\eta_c'$ candidate.
- New results on exclusive states produced in $J/\psi$ radiative transitions. The new results are primarily from the Crystal Ball, but some Mark II results are presented also. Two candidates for gluonium states have been observed.

Other recent results from SPEAR are mentioned below, but will not be discussed in this talk.

- New measurements of $\psi' \to \gamma\gamma$ $J/\psi$ from both the Mark II[3] and Crystal Ball[4,5] experiments.
- Limits from the Crystal Ball[6] on $J/\psi \to \gamma$ + axion.
- New measurements of the total hadronic cross section at center-of-mass energies between 5 and 7 GeV from the Crystal Ball.[7]

---

(Invited talk presented at the 1981 International Symposium on Lepton and Photon Interactions at High Energies, Bonn, Germany, August 24-29, 1981.)

*Work supported by the Department of Energy, contract DE-AC03-76SF00515.

- Analysis of resonance structure in two-photon production[8] of $\pi\pi$, $4\pi$, and $\eta\pi$ from the Mark II and Crystal Ball.
- Measurement by the Mark II of the Cabibbo suppressed decay $\tau \to K\nu_\tau$.[6]
- New limits from the Mark II[9] on free quark production in $e^+e^-$ annihilations.

Before proceeding to the discussion of the physics results, I will point out the main features of the Crystal Ball and Mark II detectors. The Crystal Ball detector, shown in Fig. 1, has just completed its third year of data taking at SPEAR. The main feature of this non-magnetic detector is the large solid angle and excellent electromagnetic energy resolution provided by the NaI(Tℓ) crystals. Typical photon energy and angular resolutions obtained by the Crystal Ball are $\sigma_E/E \approx 2.8\%/E^{\frac{1}{4}}$ (E in GeV) and $\sigma_\alpha \approx$ 1-2 degrees. Magnetostrictive spark chambers and multiwire proportional chambers around the beam pipe allow measurement of charged particle trajectories with typical polar and azimuthal angular resolutions of $\sigma_\theta \approx 2$ degrees and $\sigma_\phi \approx$ 2-5 mr. Charged particle momentum measurements cannot be made.

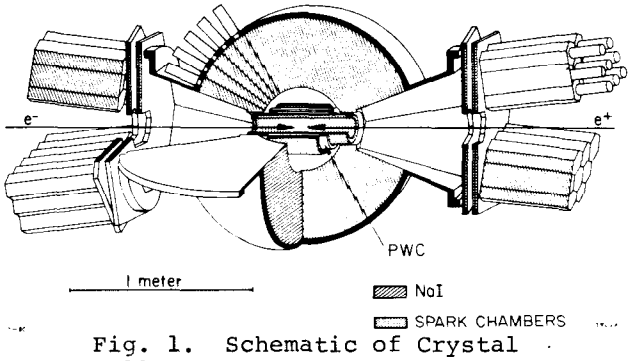

Fig. 1. Schematic of Crystal Ball Detector.

The Mark II detector[10] was moved from SPEAR to PEP two years ago. It is a large solid angle magnetic spectrometer which utilizes a drift chamber system for charged particle tracking and momentum measurements and lead-liquid argon shower counters for photon energy and angle measurements. The photon energy resolution is $\sigma_E/E \approx 12\%/E^{\frac{1}{2}}$ (E in GeV) and the charged particle momentum resolution is $\sigma_p/p \approx [(.005p)^2 + (.015)^2]^{\frac{1}{2}}$ (p in GeV).

## II. $\psi'$ INCLUSIVE PHOTON MEASUREMENTS

Figure 2 shows the inclusive photon spectrum at the $\psi'$ from the Crystal Ball. This spectrum is from a preliminary analysis of approximately half of the 1.78 x $10^6$ produced $\psi'$ events in the data sample. Severe cuts have been made to the data to enhance structure. First, all photons are required to have $|\cos\theta_\gamma| < 0.85$, where $\theta_\gamma$ is the angle between the photon and the beam direction. The cosine of the angle between each photon and any charged particle is required to be less than 0.9. Pairs of $\gamma$'s with invariant mass consistent with the mass of the $\pi^o$ have been eliminated. Finally, the lateral shower energy deposition in the NaI crystals is required to be consistent with a single electromagnetic shower. This "pattern cut" removes minimum ionizing charged particles which were not tagged by the tracking chambers, spurious energy deposits resulting from interacting charged particles, and high energy $\pi^o$'s in which the electromagnetic showers from the two photons from the $\pi^o$ decay overlap.

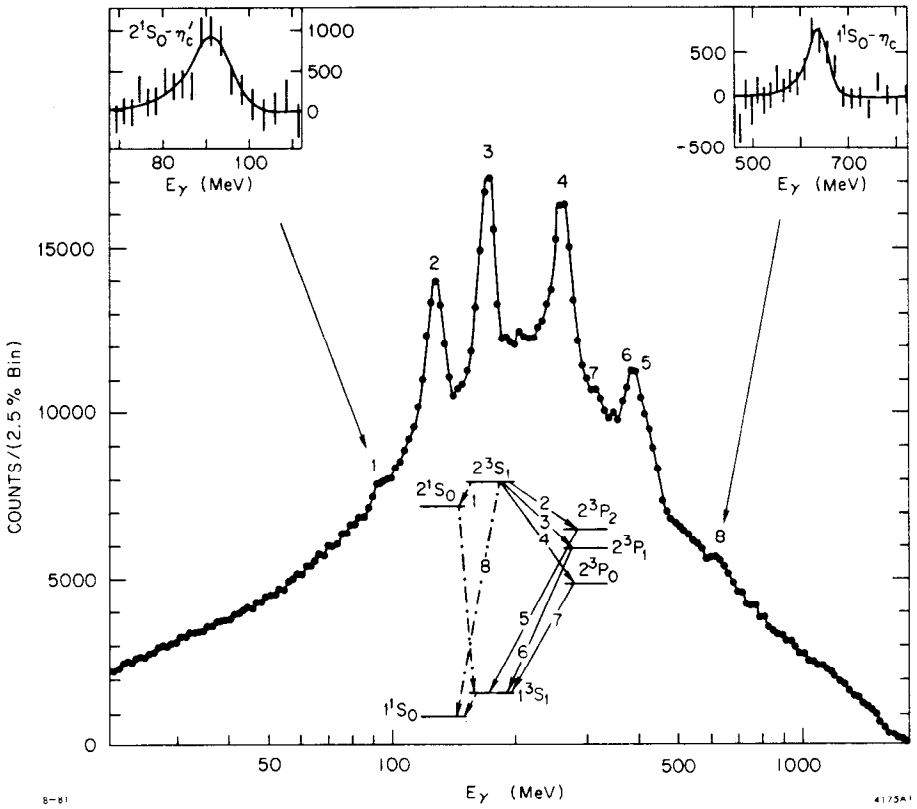


Fig. 2. Inclusive γ spectrum at the ψ'. Cuts are described in text. Lower insert shows charmonium level diagram. Upper inserts show γ distributions in the $\eta_c'$ and $\eta_c$ regions. (Crystal Ball)

As seen by examination of the charmonium level diagram insert in Fig. 2, this single spectrum reveals essentially all of charmonium spectroscopy. The peaks labeled 2, 3, and 4 correspond to transitions from the ψ' to the $\chi_2$, $\chi_1$, and $\chi_0$. Peaks 5, 6, and 7 show the locations of the $\chi_2$, $\chi_1$, and $\chi_0$ transitions to the J/ψ. (The $\chi_0$ transition is not observed because of its small branching ratio.) 8 shows the location of the transition from the ψ' to the $\eta_c$.[11,12] Finally, the small peak labeled 1 shows the transition from the ψ' to the $\eta_c'$ candidate state. The inserts[13] in the upper left and right corners show expanded views of the photon energy spectrum in the regions of the $\eta_c'$ and $\eta_c$ transitions.

Before presenting the results on the $\eta_c'$, new results on inclusive measurements of the χ and $\eta_c$ transitions will be presented. This is important in establishing that small signals from the ψ' inclusive photon spectrum can be reliably extracted from the Crystal Ball data.

A. $\psi' \to \gamma J/\psi$; $\psi' \to \gamma\gamma J/\psi$

Figure 3 shows four different inclusive spectra at the ψ'.[14] In Fig. 3(a), the observed energy of all charged and neutral particles with $|\cos\theta| < 0.85$ is shown. Clearly evident are peaks at 200 MeV resulting from minimum ionizing charged particles and at the beam energy due to Bhabha events. The χ lines do

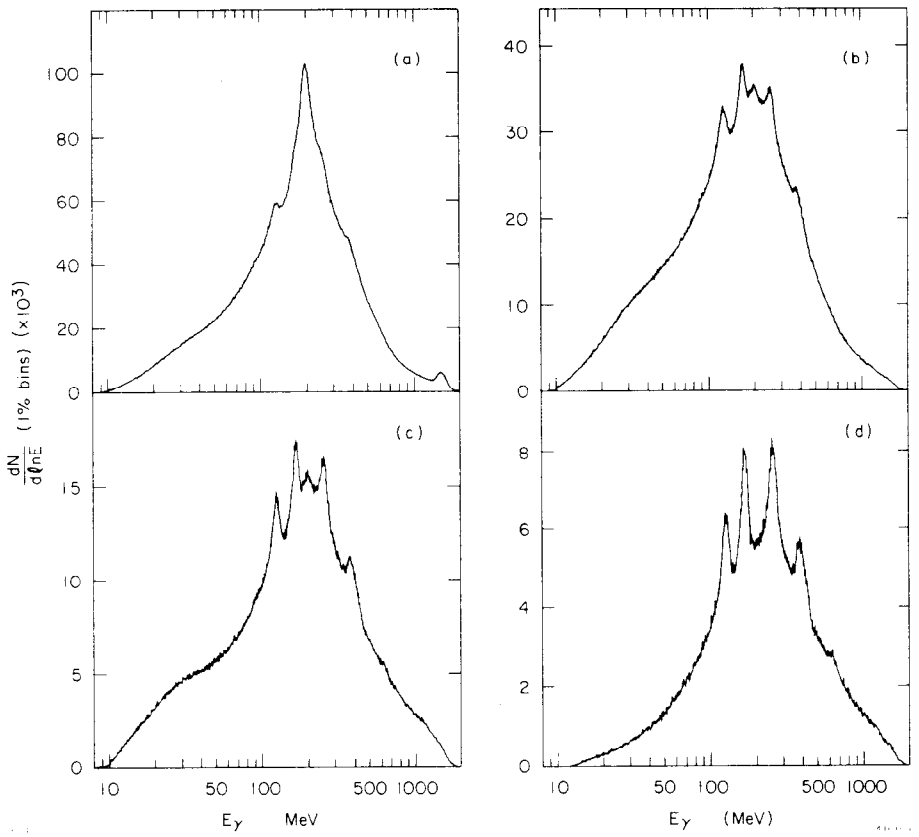


Fig. 3. Inclusive $\gamma$ spectra at the $\psi'$ a) for all particles, b) after elimination of identified charged particles, c) after $\pi^o$ subtraction, and d) after pattern cuts. (Crystal Ball)

not show up very strongly. Figure 3(b) shows the spectrum after elimination of identified charged particles. The $\chi$ lines are clear but there is still a remnant of the minimum ionizing peak. Figure 3(c) shows the spectrum after $\pi^o$ subtraction. Finally, after making the pattern cuts described above, one obtains the distribution shown in Fig. 3(d). There is no evidence of a minimum ionizing peak.

In order to extract branching ratios for the $\chi$ lines, fits were made to each of the distributions shown in Fig. 3. The structures in the spectra were parameterized as Breit-Wigner functions convoluted with the NaI line shape.[15] The background was parameterized in terms of three contributions: charged particle punch through, limited phase space photons from $\psi' \to \eta\ J/\psi$ and $\psi' \to \pi^o\pi^o\ J/\psi$, and a smooth polynomial background to account for the remaining photons. The charged particle punch through contribution (except for normalization) was determined from the tagged charged particle distribution. The limited phase space photons were determined by Monte Carlo analysis.

Figure 4(a) shows the result of the fit to the spectrum in Fig. 3(a). Also shown is the distribution after background subtraction. Similar distributions for the spectrum in Fig. 3(d) are shown in Fig. 4(b). The branching ratios for $\psi' \to \gamma\chi_J$, as determined from each of the four distributions in Fig. 3, are shown graphically in Fig. 5 (the top half of the plot). The four measurements of each

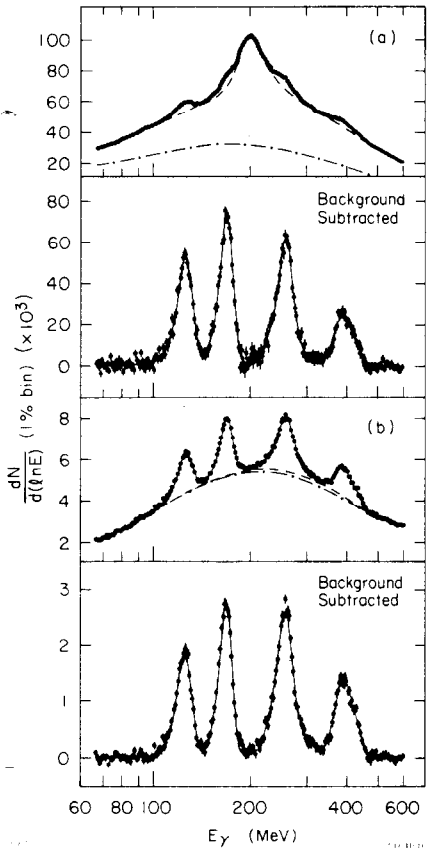


Fig. 4. Inclusive γ spectra at the ψ' a) for all particles and b) after pattern cuts. Also shown are distributions after background subtraction. Curves show best fits to spectra (solid), background (dashed), and polynomial component of background (dashed-dotted). (Crystal Ball)

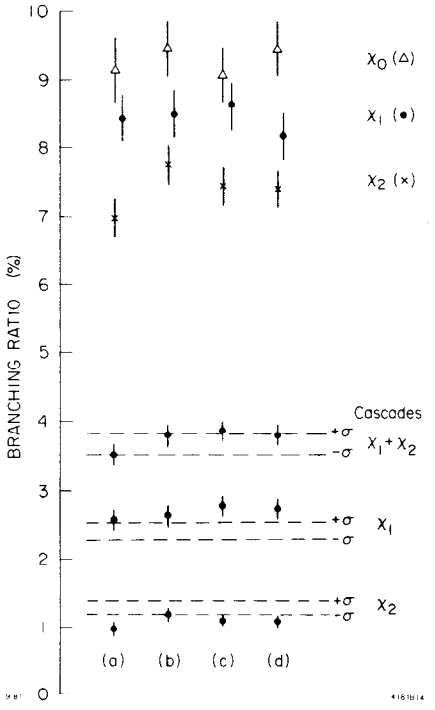


Fig. 5. Measured inclusive branching ratios as determined from spectra a) for all particles, b) for neutrals only, c) after $\pi^0$ subtraction, and d) after pattern cuts. Data points in top half of plot are for $\psi' \to \gamma \chi_J$. Data points in bottom half of plot are product branching ratios for cascade process $\psi' \to \gamma\chi_J$, $\chi_J \to \gamma J/\psi$. Dashed lines are ±1σ limits from the exclusive process $\psi' \to \gamma\gamma J/\psi$, $J/\psi \to \ell^+\ell^-$. (Crystal Ball)

branching ratio are in good agreement. The best values for these branching ratios are given in Table I.

In Fig. 4, the fourth (highest energy) peak in each distribution is due to the two transitions $\chi_1 \to \gamma J/\psi$ and $\chi_2 \to \gamma J/\psi$ (i.e., the peak results from photons produced in the second step of the double cascade process $\psi' \to \gamma \chi_J$, $\chi_J \to \gamma J/\psi$).

Table I. $B(\psi' \to \gamma \chi_J)$.

| $\chi_J$ | $B(\psi' \to \gamma \chi_J)$ (%) | | |
|---|---|---|---|
| | Crystal Ball | $MP^2S^3D$ [a] | Theory[b] |
| $\chi_0$ | 9.3 ± 0.4 ± 1.4[c] | 7.2 ± 2.3 | 20 ± 4 |
| $\chi_1$ | 8.4 ± 0.4 ± 1.3[c] | 7.1 ± 1.9 | 16 ± 3 |
| $\chi_2$ | 7.4 ± 0.4 ± 1.1[c] | 7.0 ± 2.0 | 11 ± 2 |

[a] Ref. 16. [b] Ref. 17.

[c] First error is statistical; second is systematic.

Extraction of these branching ratios requires a detailed understanding of the detector and detection efficiencies for photons. The product branching ratios $B(\psi' \to \gamma\chi_J) \times B(\chi_J \to \gamma\ J/\psi)$ for the $\chi_1$ and the $\chi_2$ (as well as the sum of the two), as determined from each of the four spectra, are shown in the bottom half of Fig. 5. Not only are the four measurements in good agreement in each case, but the measurements agree well with measurements determined independently by the Crystal Ball[5] from the process

$$\psi' \to \gamma\gamma\ J/\psi,\ J/\psi \to \ell^+\ell^- ,$$

where $\ell$ is either e or $\mu$. These measurements are summarized in Table II. For completeness, the widths of the $\chi$ states, as determined from these fits to the inclusive spectra, are given in Table III.

Table II. $B(\psi' \to \gamma\chi_J) \times B(\chi_J \to \gamma\ J/\psi)$

| $\chi_J$ | $B(\psi' \to \gamma\chi_J) \times B(\chi_J \to \gamma\ J/\psi)$ (%) | | |
|---|---|---|---|
| | Crystal Ball (inclusive) | Crystal Ball[a] (exclusive) | World Average[b] (exclusive) |
| $\chi_1$ | 2.65 ± 0.16 ± 0.40[c] | 2.38 ± 0.40 | 2.34 ± 0.21 |
| $\chi_2$ | 1.07 ± 0.10 ± 0.16[c] | 1.26 ± 0.22 | 1.16 ± 0.12 |

[a] Ref. 5.
[b] Ref. 18.
[c] First error is statistical; second is systematic.

B. $\psi' \to \gamma\ \eta_c$

Figure 6(b) shows the inclusive photon spectrum at the $\psi'$ without $\pi^0$ subtraction but after making pattern cuts. The spectrum in the region of the $\eta_c$ transition (approximately 500-900 MeV) is shown plotted with a linear energy scale in Fig. 7(a). A fit to this spectrum consisting of a Gaussian plus a polynomial background gives $E_\gamma$ = 638 ± 4 MeV for the photon energy. This corresponds to a mass for the $\eta_c$ of M = 2978 ± 5 MeV. The background subtracted distribution is shown in Fig. 7(b).

Table III. Widths of $\chi$ States

| $\chi_J$ | $\Gamma$ (MeV) |
|---|---|
| $\chi_0$ | 16.3 ± 3.6 |
| $\chi_1$ | <1.5[a] |
| $\chi_2$ | 1.8 ± 0.6 |

[a] 90% confidence level upper limit.

The authenticity of the signal is established by the fact that the $\eta_c$ has also been observed in inclusive transitions from the $J/\psi$[11] and in exclusive final states[11,12] from both the $J/\psi$ and the $\psi'$. A simultaneous fit to the $\eta_c$ signals observed by the Crystal Ball in both the $\psi'$ and $J/\psi$ (not shown here) inclusive photon distributions gives a mass of M = 2984 ± 4 MeV. New results on the $\eta_c$ are summarized in Table IV.

Table IV. New Results on the $\eta_c$

$M = 2984 \pm 4$ MeV

$\Gamma = 12.4 \pm 4.1$ MeV

$B(\psi' \to \gamma\eta_c) = (0.28 \pm 0.08)\%$

$B(J/\psi \to \gamma\eta_c) = (1.13 \pm 0.33)\%$

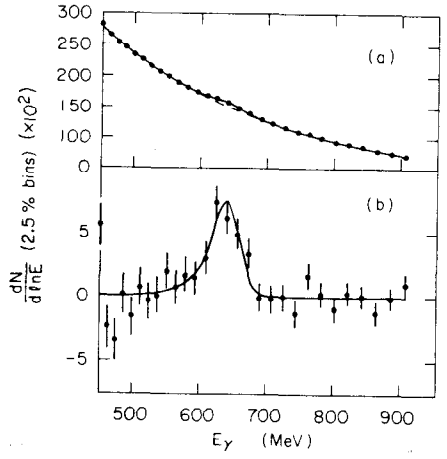


Fig. 7. Inclusive $\gamma$ spectrum at the $\psi'$ in the region of the $\eta_c$ transition a) before and b) after background subtraction. Curves represent best fit to a Gaussian plus a polynomial background. (Crystal Ball)

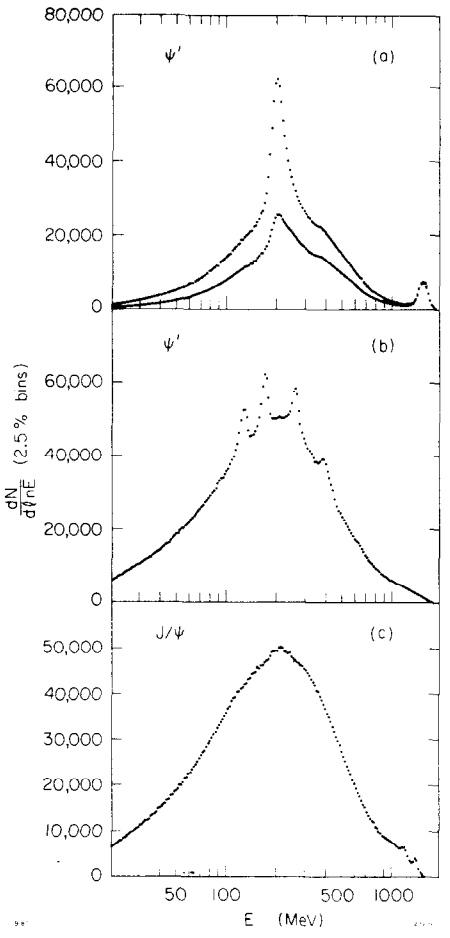


Fig. 6. a) Inclusive charged particle spectrum at the $\psi'$; b) inclusive $\gamma$ spectrum at the $\psi'$; and c) inclusive $\gamma$ spectrum at the J/$\psi$. Two distributions in (a) correspond to all charged tracks and only those charged tracks satisfying pattern cuts. (Crystal Ball)

C. $\psi' \to \gamma\eta_c'$

This analysis is based on the same spectrum as was used in the $\eta_c$ analysis [See Fig. 6(b)]. The spectrum between 60 and 110 MeV is shown plotted with a linear scale in Fig. 8(a). The curves show the best fit to the distribution based on a Gaussian plus a polynomial background. Figure 8(b) shows the signal after background subtraction. The statistical significance of the signal is 4.4 $\sigma$. The fit determines the energy of the photon to be $E_\gamma = 91 \pm 1$ MeV (statistical error only). This corresponds to a mass for the $\eta_c'$ candidate of $M = 3592 \pm 5$ MeV, where the error now includes the estimated systematic uncertainty. The width of the peak is consistent with the known energy resolution of the NaI. This leads to a 95% confidence level upper limit on the width of the state of 8 MeV. A preliminary estimate of the branching ratio is (0.2-1.3)%. (These are 95% confidence level limits.) This is consistent with the theoretical prediction[17] of approximately ½% for the transition from the $\psi'$ to an $\eta_c'$ with this mass. These results are summarized in Table V.

As one has to worry about correlations between the signal and the background for such small signals, an alternate approach was taken. First, the background

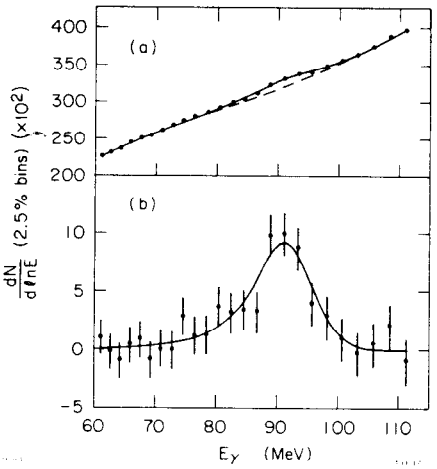


Fig. 8. Inclusive $\gamma$ spectrum at the $\psi'$ in the region of the transition to the $\eta_c'$ candidate a) before and b) after background subtraction. Curves represent best fit to a Gaussian plus a polynomial background. (Crystal Ball)

Table V. Parameters of the $\eta_c'$ Candidate

$M = 3592 \pm 5$ MeV

$\Gamma < 8$ MeV (95% C.L.)

$B(\psi' \to \gamma\eta_c') = (0.2 - 1.3)\%$ (95% C.L.)

Significance of signal = 4.4 $\sigma$

distribution in the region outside the signal region was fitted. Then, with the background fixed, the distribution inside the signal region was fitted with a Gaussian plus the background. The parameters of the signal (a 6.1 $\sigma$ effect in this case) were found to be consistent with the results of the previous analysis.

The previous discussions have established that the signal is probably real. However, it is possible that there is some background effect which might produce a signal at 90 MeV in the photon energy spectrum. Possible backgrounds which might simulate a signal are unidentified charged particles, exclusive decays of the $\psi'$ containing photons, and unknown hardware or software effects. Each of these possibilities has been examined in detail.

If the signal somehow resulted from misidentified charged particles, there should be a very large signal in the inclusive tagged charged particle spectrum. Figure 6(a) shows the charged particle energy spectrum at the $\psi'$ after invoking the same pattern cuts as were used in the analysis of the $\eta_c'$ candidate. There is no evidence for a signal near 90 MeV.

Exclusive final states which could potentially simulate a signal include

$$\psi' \to \pi^o\pi^o\, J/\psi$$
$$\psi' \to \eta\, J/\psi$$
$$\psi' \to J/\psi + X,\ J/\psi \to \gamma\eta_c\ .$$

These processes have been studied and all give broad photon spectra, and hence could not lead to a narrow signal near 90 MeV.

Two checks were made to establish that the signal was not due to an unknown hardware or software effect. First, it it were, it is expected that the effect would be independent of center-of-mass energy. An analysis of the inclusive photon spectrum at the $J/\psi$ based on over two million produced $J/\psi$ events shows no evidence for a signal near 90 MeV [see Fig. 6(c)]. Second, the data were partitioned according to which part of the detector the photon was observed in, and during which part of the running time the data were taken. As shown in Fig. 9, there is no evidence for any position- or time-dependent correlations.

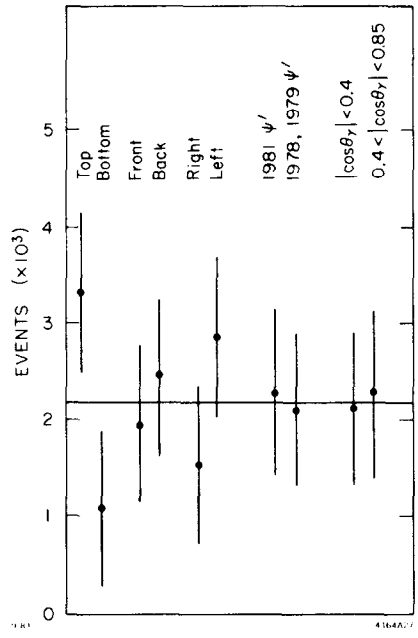


Fig. 9. Number of observed $\eta_c'$ candidates as a function of time and position in the detector. (Crystal Ball)

Although all evidence indicates that the signal is real, identification of this state as the $\eta_c'$ is based only on the expectation that such a state should exist with approximately the measured mass and branching ratio. Observation of exclusive decays of this state would provide constraints on the quantum numbers, and hopefully establish the identity of the state.

## III. OBSERVATION OF POSSIBLE GLUONIUM STATES IN J/ψ RADIATIVE DECAYS

The existence of gluonium resonances,[19] bound states of two or more gluons, is expected within the framework of QCD. Most estimates of the masses of the lowest lying states are below 2 GeV, and hence easily accessible to present experiments. According to leading-order QCD predictions, the hadronic decays of heavy quark-antiquark $^3S$ states (such as the J/ψ) proceed via annihilation of the $Q\bar{Q}$ system into three gluons as shown in Fig. 10(a). Although this process might seem to be ideal for production of gluonium states, it is not. Each pair of gluons is a color-octet state since it is recoiling against a single color-octet gluon. On the other hand, if a photon is radiated from the heavy quark line before annihilation, as

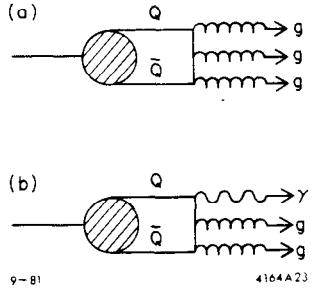


Fig. 10. Leading-order QCD diagrams for the decay of the J/ψ into a) hadrons and b) a direct photon plus hadrons.

in Fig. 10(b), the recoiling 2-gluon system is a color singlet. This process is expected to be a good source of gluonium states. For the J/ψ, the ratio of γgg production to 3-gluon production is predicted to be 0.13 (based on the leading-order calculation[20]).

A. $\underline{J/\psi \to \gamma\iota(1440)}$

The process

$$J/\psi \to \gamma\iota(1440) \qquad (1)$$

was first observed by the Mark II[21] in the final state

$$J/\psi \to \gamma K_S K^{\pm}\pi^{\mp} \quad . \qquad (2)$$

The $K_S K^{\pm}\pi^{\mp}$ invariant mass for events which satisfy constrained fits to process (2) is shown in Fig. 11. A peak near 1440 MeV is observed which is significantly enhanced relative to the background if the $K\bar{K}$ invariant mass is required to be small ($M_{K\bar{K}}$ < 1050 MeV for the shaded region in Fig. 11). This state was originally identified as the E(1420) meson[22] which has been previously observed in πp and $\bar{p}p$ interactions. The measured parameters of this state are given in Table VI.

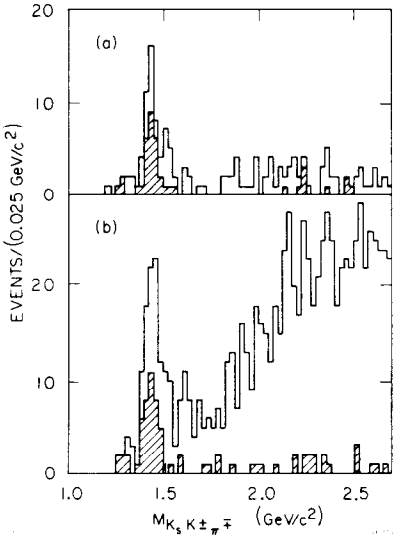


Fig. 11. $K_S K^{\pm}\pi^{\mp}$ invariant mass distribution for a) events with and b) events without an observed γ from the process $J/\psi \to \gamma K_S K^{\pm}\pi^{\mp}$. Shaded regions have requirement that $M_{K\bar{K}}$ < 1050 MeV. (Mark II)

Process (1) has also been observed by the Crystal Ball. Figure 12 shows the $K^+K^-\pi^0$ invariant mass distribution for events which satisfy constrained fits[23] to the process

$$J/\psi \to \gamma K^+K^-\pi^0$$

This analysis is based on over two million produced J/ψ events. The shaded region corresponds to events with $M_{K\bar{K}}$ < 1125 MeV. Figure 13 shows the shaded distribution from Fig. 12 in 10 MeV bins. The curve is a Breit-Wigner fit to the mass

Table VI. ι(1440) Parameters

| Parameter | Experimental Measurement | |
|---|---|---|
| | Mark II[a] | Crystal Ball |
| M | $1440 \begin{smallmatrix}+10\\-15\end{smallmatrix}$ Mev | $1440 \begin{smallmatrix}+20\\-15\end{smallmatrix}$ MeV |
| Γ | $50 \begin{smallmatrix}+30\\-20\end{smallmatrix}$ MeV | $60 \begin{smallmatrix}+20\\-30\end{smallmatrix}$ Mev |
| $B(J/\psi \to \gamma\iota) \times B(\iota \to K\bar{K}\pi)$ | $(4.3 \pm 1.7) \times 10^{-3}$ [b] | $(4.0 \pm 1.2) \times 10^{-3}$ |

[a] Ref. 21.

[b] This product branching ratio has been corrected by me to account for the efficiency correction required under the spin 0 hypothesis.

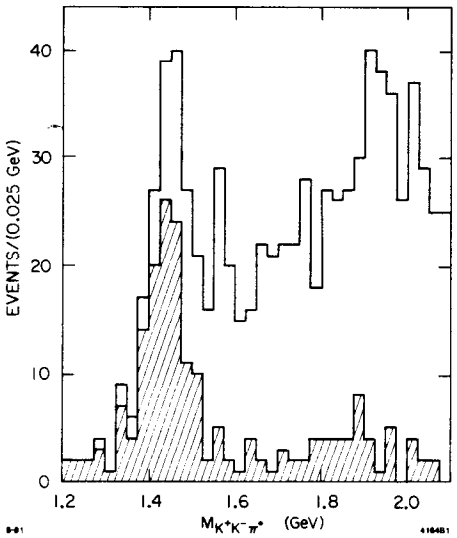


Fig. 12. $K^+K^-\pi^0$ invariant mass distribution for events consistent with the hypothesis $J/\psi \to \gamma K^+K^-\pi^0$. Shaded region has the requirement $M_{K\bar{K}} < 1125$ MeV. (Crystal Ball)

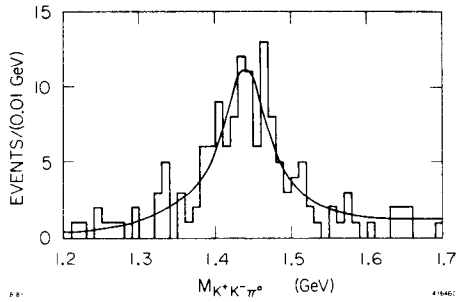


Fig. 13. $K^+K^-\pi^0$ invariant mass distribution with $M_{K\bar{K}} < 1125$ MeV. Curve represents fit to distribution. (Crystal Ball)

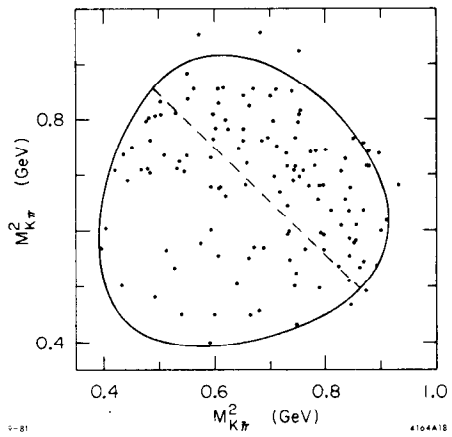


Fig. 14. $K^+K^-\pi^0$ Dalitz plot for events with $1400 \leq M_{K\bar{K}\pi} < 1500$ MeV. Solid curve shows boundary for $M_{K\bar{K}\pi} = 1450$ MeV. Dashed line shows $M_{K\bar{K}} = 1125$ MeV. (Crystal Ball)

distribution. The measured parameters of the ι as determined by the Crystal Ball group are also given in Table VI. The mass and width were determined from the distribution in Fig. 13, although the parameters determined from the full distribution in Fig. 12 give consistent results.

The $K\bar{K}\pi$ Dalitz plot from the Crystal Ball is shown in Fig. 14. A low $K\bar{K}$ mass enhancement (in the upper right corner of the plot) is evident. This enhancement has been associated with the $\delta(980)\pi$ decay of the resonance. No evidence for K* bands, which would indicate a $K^*\bar{K}$ + c.c. decay, is observed, although the situation is potentially confusing because of the limited phase space available for the decay and the fact that the K* bands overlap in the region of the δ. The Mark II results are consistent with this. They find the ι to decay primarily into $\delta\pi$.

From the beginning, interest in this state has centered around the relatively large branching ratio for this transition compared to branching ratios for other radiative transitions from the J/ψ. This was particularly interesting considering the relative obscurity of the E(1420), the state with which the ι was originally identified, in hadronic interactions. These facts motivated the suggestion that this state might be a gluonium resonance.[24] Many arguments for[25] and against[26] this hypothesis have been made. New results to be presented here on the spin of the ι from the Crystal Ball group show that the ι is not to be identified with the E(1420). This provides additional support for the gluonium hypothesis.

Before discussing the Crystal Ball spin analysis of the ι(1440), I will review the status of the E(1420). The best estimate of the mass[22] is $M_E = 1418 \pm 10$ Mev. This is somewhat lower than, but not inconsistent with, the average of the Mark II and Crystal Ball measurements of the ι mass, $M_\iota = 1440 \pm 10$ MeV. Figure 15 summarizes the various mass measurements of the E and ι along with a Gaussian ideogram of the E mass measurements. The widths of the E ($\Gamma_E = 50 \pm 10$ MeV) and the ι ($\Gamma_\iota = 55 \pm 20$ Mev) are also consistent. Thus the mass and width measurements of the ι do not clearly identify it as a different state than the E.

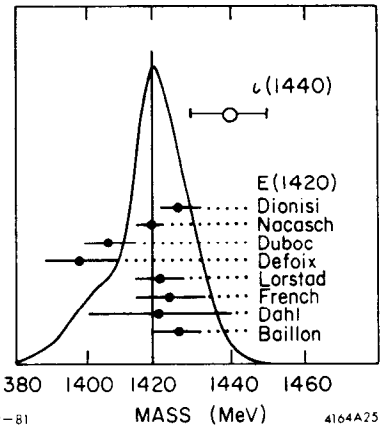

Fig. 15. Summary of E and ι mass measurements.

The spin of the E was established in an experiment which analyzed the reaction

$$\pi^- p \to K_S K^\pm \pi^\mp n$$

at 3.95 GeV/c.[27] The results of a partial-wave analysis of the $K\bar{K}\pi$ system determined $J^{PC} = 1^{++}$ for the E, thus making it the SU(3) nonet partner of the D(1285) and the $A_1$. However, a previous experiment[28] which looked at $\bar{p}p \to E\pi\pi$ determined the spin-parity of the E to be $0^-$. Although these earlier results were not conclusive, they provide some support for the hypothesis that there is more than one state with mass near 1400 MeV.[29] An additional result of the partial-wave analysis of Dionisi et al., is that the E decays primarily into $K^*\bar{K}$ + c.c. with

$$\frac{B(E \to K^*\bar{K} + \text{c.c.})}{B(E \to K^*\bar{K} + \text{c.c.} + \delta\pi)} = 0.86 \pm 0.12 \quad .$$

The spin of the ι(1440) was determined from a partial-wave analysis of the Crystal Ball data. Contributions from five partial waves were included:[30]

1. $K\bar{K}\pi$ flat (phase space)
2. $\delta^0\pi^0 - 0^-$
3. $\delta^0\pi^0 - 1^+$
4. $K^*\bar{K}$ + c.c. - $0^-$
5. $K^*\bar{K}$ + c.c. - $1^+$

Contributions from all partial waves except $K\bar{K}\pi$ flat were allowed to interfere with arbitrary phase. The $K\bar{K}\pi$ flat contribution was assumed to be incoherent. The full angular decay distributions in each case were included in the amplitudes. The ι and K* helicities were allowed to vary in the fits. The δ and K* parameters were taken to be the standard values.[22] In other words, a standard isobar analysis in the Berkeley tradition[31] was done.

The analysis was done for events with $K\bar{K}\pi$ masses between 1300 and 1800 MeV. The data were divided into five bins of 100 MeV each. The standard procedure of eliminating those partial waves which do not contribute significantly to the likelihood was utilized (i.e., the number of events contributed by a given partial wave

was required to be larger than the error on that number). The only significant contributions were from $K\bar{K}\pi$ flat, $\delta^0\pi^0 - 0^-$, and $K^*\bar{K}$ + c.c. - $1^+$. These contributions, corrected for detection efficiency, are shown as a function of $K\bar{K}\pi$ mass in Fig. 16. The $K^*\bar{K}$ + c.c. - $1^+$ contribution is relatively small and independent of mass. On the other hand, the $\delta\pi - 0^-$ contribution shows clear evidence for resonant structure in the $\iota$ signal region ($1400 \leq M_{K\bar{K}\pi} < 1500$ MeV). This establishes the spin-parity of the $\iota$ as $0^-$. (The C-parity is required to be even because of the production mechanism.) In addition, contrary to the case of the E(1420), the principal decay of the $\iota$ is into $\delta\pi$ and

$$\frac{B(\iota \to K^*\bar{K} + \text{c.c.})}{B(\iota \to K^*\bar{K} + \text{c.c.} + \delta\pi)} < 0.25 \quad (90\% \text{ C.L.})$$

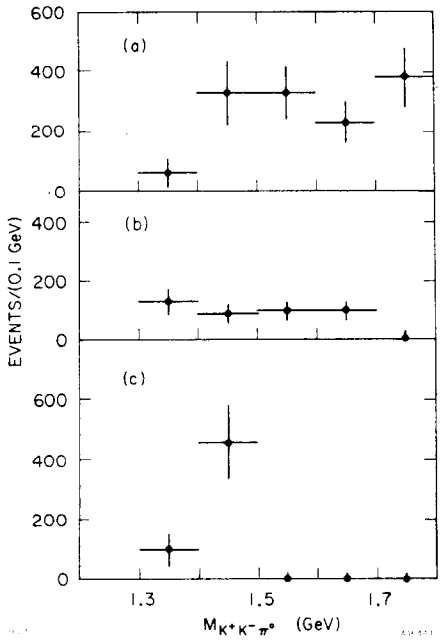


Fig. 16. Partial-wave contributions as a function of $K\bar{K}\pi$ mass for a) $K\bar{K}\pi$ flat, b) $K^*\bar{K}$ + c.c. - $1^+$, and c) $\delta\pi - 0^-$. (Crystal Ball)

As a number of assumptions went into the partial-wave analysis, in particular, only a limited number of partial waves were considered; checks were made to show that the results of the analysis were valid. First, maximum likelihood fits were made to the restricted hypothesis that in each mass interval, only one partial-wave contribution in addition to the flat contribution was allowed. The relative probabilities resulting from fits to the data in the signal region ($1400 \leq M_{K\bar{K}\pi} < 1500$ MeV) are given in Table VII. Note that compared to the $\delta\pi - 0^-$ hypothesis, the next best hypothesis ($K^*\bar{K}$ + c.c. - $1^+$) has a relative probability of only 1%. This establishes that there is not a strong correlation between the $\delta\pi$ and $K^*\bar{K}$ + c.c. amplitudes.

Table VII. Relative Partial-Wave Probabilities ($1400 \leq M_{K\bar{K}\pi} < 1500$ MeV)

| Partial-Wave Contribution | Relative Probability |
|---|---|
| flat + $\delta\pi - 0^-$ | 1.0 |
| flat + $\delta\pi - 1^+$ | 0.006 |
| flat + $K^*\bar{K}$ + c.c. - $0^-$ | $10^{-7}$ |
| flat + $K^*\bar{K}$ + c.c. - $1^+$ | 0.01 |

It was also checked that the mass distributions of the di-particle systems were in agreement with Monte Carlo distributions based on the measured partial-wave contributions. Figure 17 shows the $K^+K^-$ invariant mass distribution for events with $K\bar{K}\pi$ invariant mass between 1400 and 1500 MeV. The distribution rises sharply at threshold due to the large $\delta$ contribution. This same behavior was previously observed in the Mark II $K_sK^\pm$ invariant mass distribution (see Fig. 18). In both the Crystal Ball and Mark II mass distributions, the expected phase space distribution is in disagreement with the data. The phase space distribution fails to duplicate the threshold enhancement and also predicts too many events at high $K\bar{K}$ mass. The best fit to the Crystal Ball data (which includes the flat, $K^*\bar{K}$ + c.c.,

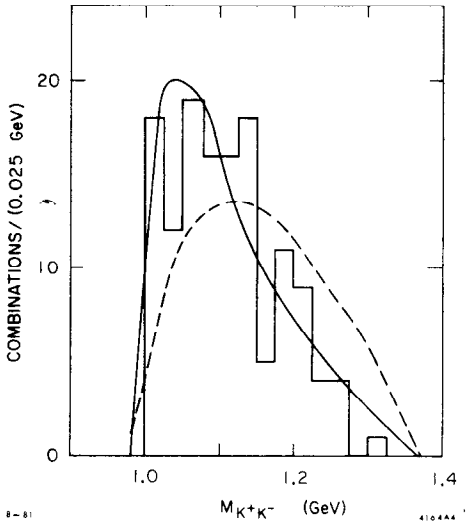


Fig. 17. $K^+K^-$ invariant mass distribution ($1400 \leq M_{KK\pi} < 1500$ MeV). Solid curve represents results of best fit from partial-wave analysis. Dashed curve represents expected phase space distribution. (Crystal Ball)

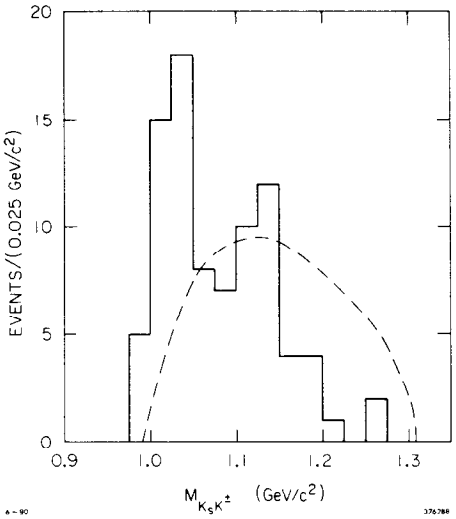


Fig. 18. $K_SK^\pm$ invariant mass distribution ($1375 \leq M_{K\bar{K}\pi} < 1500$ MeV). Dashed curve represents expected space distribution. (Mark II)

and $\delta\pi$ contributions as determined from the partial-wave analysis) is in good agreement with the mass distribution, as shown by the curve in Fig. 17.

The $K^+K^-$ invariant mass distribution for events outside the signal region looks qualitatively different than the distribution for events inside the signal region. Figure 19 shows this distribution for events in the $K\bar{K}\pi$ mass interval from 1500 to 1600 MeV. There is no evidence for the sharp rise at threshold as seen in Figs. 17 and 18, i.e., there is no evidence for $\delta$ production outside the $\iota(1440)$ signal region.

As the parametrization of the $\delta(980)$ is subject to some uncertainty, it was checked that the basic results were insensitive to the parameterization. This is important as the $\delta$ Breit-Wigner parameters were determined from fits to the $\delta \to \eta\pi$ decay mode and it has never been established that what is referred to as the $\delta$ in the $K\bar{K}$ channel is the same object.[32] Fits which were made with wider $\delta$'s (e.g., $\Gamma = 70$ MeV rather than 50 MeV) resulted in slightly more $\delta\pi$ contribution and slightly less phase space contribution (for the signal region) but with essentially no change in the $K^*\bar{K}$ + c.c. contribution. Thus, changing the parametrization of the $\delta$ results in trade-offs between the phase space and $\delta\pi$ contributions. The seeming excess of phase space events for $1400 \leq M_{K\bar{K}\pi} < 1500$ MeV in Fig. 16 is most likely a result of the $\delta$ parametrization.

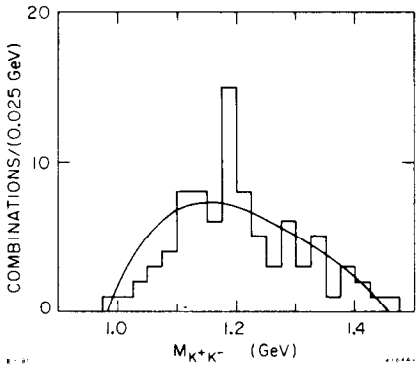


Fig. 19. $K^+K^-$ invariant mass distribution ($1500 \leq M_{K\bar{K}\pi} < 1600$ MeV). Curve represents result of best fit from partial-wave analysis. (Crystal Ball)

Figure 20 shows the $K^{\pm}\pi^{O}$ invariant mass distribution from the Crystal Ball for events with $K\bar{K}\pi$ mass between 1400 and 1500 MeV. Also shown are the expected distributions for 100% phase space, 100% $K^*\bar{K}$ + c.c., 100% $\delta\pi$, and the best fit from the partial wave analysis. The best fit distribution agrees well with the data; the other distributions not so well. The poorest agreement is for 100% $K^*\bar{K}$ + c.c. where the large $K^*$ signal expected from the Monte Carlo is not observed.

If one assumes dominance of the $\delta\pi$ decay mode of the $\iota$, a spin determination can be made purely on the basis of the angular distributions in the decay. Although this is not as global an analysis as the partial-wave analysis, it provides additional checks on the results. For this analysis, a "$\delta$ cut," $M_{K^+K^-} < 1125$ MeV, was made. This cut essentially eliminates the background under the $\iota$, so that the $K\bar{K}\pi$ mass range can be increased to $1375 \lesssim M_{K\bar{K}\pi} < 1525$ MeV (see Fig. 12).

Based on very general principles, the angular distribution of the $\gamma$ in the $e^+e^-$ lab frame [see Fig. 21(a)] can be expressed as

$$W(\theta_\gamma) = 1 + \alpha \cos^2\theta_\gamma \quad , \qquad (3)$$

where $\alpha = 1$ if the $\iota$ is spin 0 and $-1 \leq \alpha \leq 1$ if the $\iota$ is not spin 0. For the particular case of spin 1, if the transition is purely E1, then $\alpha = -1/3$.[33] Figure 22 shows the $\cos\theta_\gamma$ distribution corrected for detection efficiency. A fit to the distribution for $|\cos\theta_\gamma| < 0.8$ gives $\alpha = 1.4 \pm 0.8$. This is consistent with $\alpha = 1$ (i.e., spin 0), but more than two standard deviations away from $\alpha = -1/3$. However, for a spin 1 decay with arbitrary helicity, this distribution alone does not rule out spin 1.

Similarly, if one defines $\theta_\delta$ to be the angle of the $\delta$ relative to the $\gamma$ direction in the rest frame of the $\iota$ [as in Fig. 21(b)], $W(\theta_\delta) = 1$ for spin 0 (i.e., $\alpha = 0$). Figure 23 shows the $\cos\theta_\delta$ distribution corrected for detection efficiency.

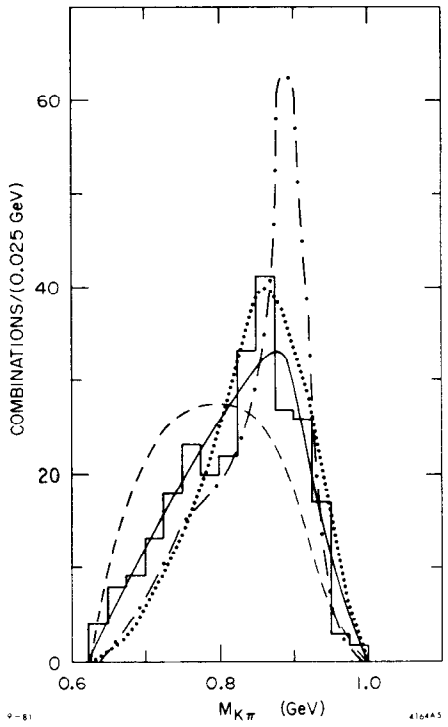


Fig. 20. $K^{\pm}\pi^{O}$ invariant mass distribution (two combinations per event) for $1400 \lesssim M_{K\bar{K}\pi} < 1500$ MeV. Curves representing best fit from partial-wave analysis (solid), phase space (dashed), 100% $\delta\pi$ - $0^-$ (dotted) and 100% $K^*\bar{K}$ + c.c. (dashed-dotted) are shown. (Crystal Ball)

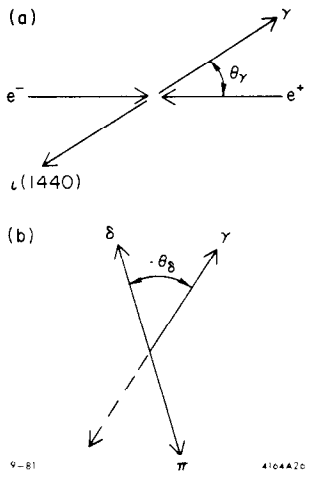


Fig. 21. Definitions of a) $\theta_\gamma$ and b) $\theta_\delta$.

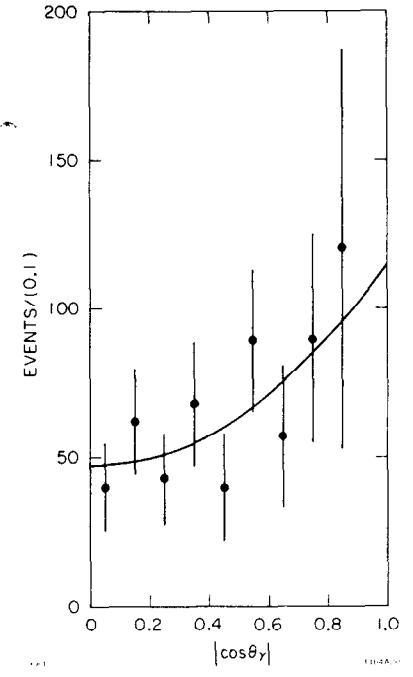


Fig. 22. $|\cos\theta_\gamma|$ distribution for $J/\psi \to \gamma\iota$ corrected for detection efficiency. Curve represents best fit. (Crystal Ball)

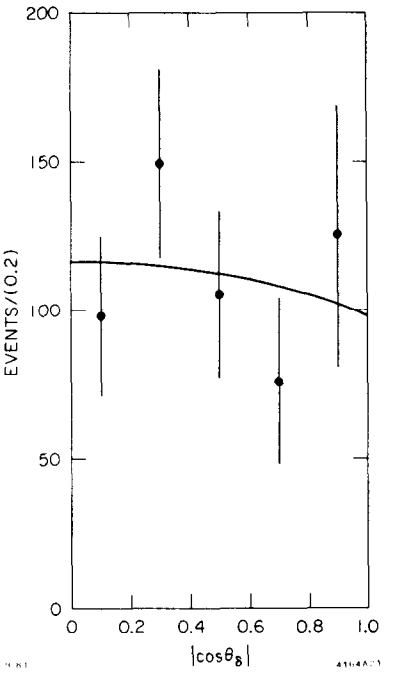


Fig. 23. $|\cos\theta_\delta|$ distribution for $\iota \to \delta\pi$ corrected for detection efficiency. Curve represents best fit. (Crystal Ball)

A fit to the distribution gives $\alpha = -0.15 \pm 0.31$, consistent with the spin 0 hypothesis.

If one does a fit to the full 3-dimensional decay distribution (a third angle $\phi_\delta$ is defined as the azimuthal angle of the $\delta$ in the $\iota$ rest frame -- see Fig. 21 -- such that $\phi_\delta = 0$ along the $e^-$ beam direction), the angular correlations allow an unambiguous determination of the spin. For spin 0, the angular distribution is given by Eq. (3). For spin 1, the distribution is[34]

$$W(\theta_\gamma, \theta_\delta, \phi_\delta) = x^2 \sin^2\theta_\gamma \sin^2\theta_\delta + (1 + \cos^2\theta_\gamma) \cos^2\theta_\delta + \tfrac{1}{2}x \sin 2\theta_\gamma \sin 2\theta_\delta \cos\phi_\delta \quad ,$$

where x is the ratio of the helicity 1 amplitude to the helicity 0 amplitude. For spin 2[34]

$$\begin{aligned} W(\theta_\gamma, \theta_\delta, \phi_\delta) = {} & 3x^2 \sin^2\theta_\gamma \sin^2 2\theta_\delta \\ & + (1 + \cos^2\theta_\gamma)\left[(3\cos^2\theta_\delta - 1)^2 + \tfrac{3}{2}y^2 \sin^4\theta_\delta\right] \\ & + \sqrt{3}x \sin 2\theta_\gamma \sin 2\theta_\delta \left[3\cos^2\theta_\delta - 1 - \tfrac{1}{2}\sqrt{6}y \sin^2\theta_\delta\right] \cos\phi_\delta \\ & + \sqrt{6}y \sin^2\theta_\gamma \sin^2\theta_\delta (3\cos^2\theta_\delta - 1) \cos 2\phi_\delta \quad , \end{aligned} \tag{4}$$

where x is defined as above and y is the ratio of the helicity 2 amplitude to the helicity 0 amplitude. The results of the maximum likelihood fits to the spin 0, 1, and 2 hypotheses are given in Table VII. Spin 0 is clearly favored.

The analyses of the Crystal Ball clearly identify the $\iota(1440)$ as a pseudoscalar meson which decays primarily (in its $K\bar{K}\pi$ decay mode) into $\delta\pi$. Clearly this state does not fit into the standard quark model ground state $0^-$ nonet. (The $\eta$ and $\eta'$ are the two isoscalar states in this nonet.) Two possibilities come to mind. The first is that the $\iota$ is a radially excited $q\bar{q}$ state. Cohen and Lipkin,[35] based on a model in which the $\eta'$ is a mixture of ground state and radially excited state wave functions, predict pseudoscalar mesons with masses near 1280 and 1500 MeV. Evidence for a pseudoscalar state with mass M = 1275 MeV and width $\Gamma$ = 70 MeV has been seen in the $\eta\pi\pi$ channel in the process[36]

$$\pi^- p \to \eta\pi\pi n \quad .$$

If one identifies this as a radially excited state, the $\iota(1440)$ is a reasonable candidate for the other state.

Table VIII. Results of Angular Distribution Analysis for $\iota \to \delta\pi$

| Spin Hypothesis | Relative Probability |
|---|---|
| 0 | 1.0 |
| 1 | $10^{-4}$ |
| 2 | 0.008 |

A more exciting possibility is that the $\iota$ is a gluonium state. A rough guide to the mass spectrum can be found by using the bag model without intergluon interactions.[37] The gluon fields can be represented as either transverse electric (TE) or transverse magnetic (TM) fields in the cavity. Table IX identifies the low-lying 2-gluon modes and the first order calculation of the masses. The $\iota$ would be identified with the $0^{-+}$ state at 1290 MeV.

Table IX. 2-Gluon Bag Model Mass Calculations

| Mode | $J^{PC}$ | Mass (MeV) |
|---|---|---|
| $(TE)^2$ | $0^{++}$, $2^{++}$ | 960 |
| (TE)(TM) | $0^{-+}$, $2^{-+}$ | 1290 |
| $(TM)^2$ | $0^{++}$, $2^{++}$ | 1590 |

B. $J/\psi \to \gamma\theta(1640)$

A new resonance has been observed by the Crystal Ball in the process

$$J/\psi \to \gamma\eta\eta \quad . \tag{5}$$

The parameters of the state, named the $\theta(1640)$, are summarized in Table X. Presently, the only known decay mode of this state is $\eta\eta$. Figure 24 shows a scatter plot of pairs of $\gamma\gamma$ invariant mass combinations for events which satisfy 3C fits[38] to the hypothesis

$$J/\psi \to 5\gamma \quad .$$

Despite the fact that there are 15 combinations per event, one sees clear evidence for the $\gamma\eta\eta$ and $\gamma\pi^0\pi^0$ final states. Figure 25 shows the projection of this plot, i.e., the $\gamma\gamma$ invariant mass distribution. The $\eta$ mass resolution is approximately 20 MeV.

Table X. $\theta(1640)$ Parameters

$M = 1640 \pm 50$ MeV

$\Gamma = 220\ ^{+100}_{-70}$ MeV

$B(J/\psi \to \gamma\theta) \times B(\theta \to \eta\eta)$
$= (4.9 \pm 1.4 \pm 1.0) \times 10^{-4}$ [a]

$B(J/\psi \to \gamma\theta) \times B(\theta \to \pi\pi)$
$< 6 \times 10^{-4}$ (90% C.L.)

$J^{PC} = 2^{++}$ favored

[a] First error is statistical; second is systematic.

Figure 26 shows the $\eta\eta$ invariant mass distribution for events which satisfy 5C fits to (5). A clear signal above a minimal background is seen at a mass of M = 1640 ± 50 MeV. The curve shows the results of a Briet-Wigner plus flat background fit to the mass distribution. The width of the resonance, $\Gamma = 220^{+100}_{-70}$ MeV, is considerably wider than the fitted mass resolution, $\sigma_M = 20$ MeV, for this channel. The product branching ratio for the process

$$J/\psi \to \gamma\theta,\ \theta \to \eta\eta$$

is $(4.9 \pm 1.4 \pm 1.0) \times 10^{-4}$, where the first error is statistical and the second is the estimated systematic uncertainty. Although this product branching ratio is nearly an order of magnitude smaller than the same number for the $\iota$, there may be other decay modes of the $\theta$ with relatively large branching ratios. The $\pi^o\pi^o$ decay of the $\theta$ has been looked for but not observed. The limit on the branching ratio is slightly larger than the measured $\eta\eta$ branching ratio, $B(J/\psi \to \gamma\theta) \times B(\theta \to \pi\pi) < 6 \times 10^{-4}$ (90% C.L.). See the next section for the $\pi^o\pi^o$ mass distribution.

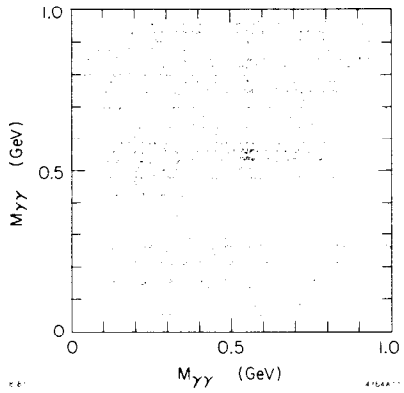


Fig. 24. $\gamma\gamma$ vs. $\gamma\gamma$ invariant mass (15 combinations per event) for events consistent with the hypothesis $J/\psi \to 5\gamma$. (Crystal Ball)

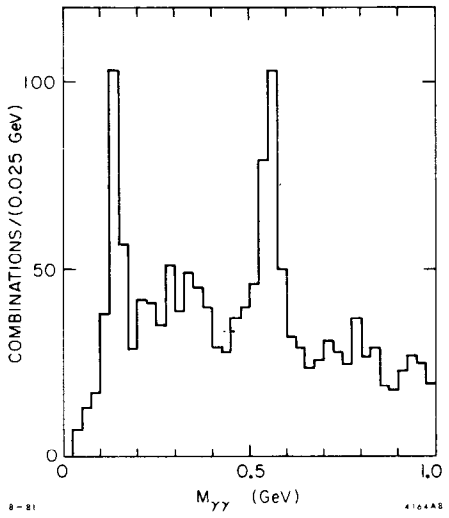


Fig. 25. $\gamma\gamma$ invariant mass distribution (10 combinations per event) for events consistent with the hypothesis $J/\psi \to 5\gamma$. (Crystal Ball)

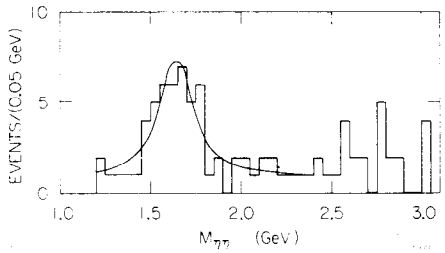


Fig. 26. $\eta\eta$ invariant mass distribution for events which satisfy fits to the hypothesis $J/\psi \to \gamma\eta\eta$. Curve shows result of fit to mass distribution. (Crystal Ball)

The fact that the θ decays into ηη and C = + (since it is produced in the radiative decay of the J/ψ) establishes that $J^{PC} = 0^{++}$ or $2^{++}$. (It is assumed that a spin of 4 or greater is very unlikely.) The Crystal Ball has done a spin analysis of the θ based on the 3-dimensional decay angular distribution in a manner similar to the ι(1440) analysis. The angular distributions for spin 0 and spin 2 are given in Eqs. (3) and (4) and the angles are defined in Fig. 21. ($\theta_\delta$ and $\phi_\delta$ should be replaced by $\theta_\eta$ and $\phi_\eta$ in all cases.) The results of the maximum likelihood fits are given in Table XI. Spin 2 is favored over spin 0. For the spin 2 hypothesis, the best fit gives $x = 0.87 \pm 0.20$ and $y = -0.64 \pm 0.39$.

Figure 27 shows the $\cos\theta_\gamma$ and $\cos\theta_\eta$ projections, compared with the results for the spin 0 and spin 2 fits. In contrast to the angular distributions shown for the ι, these distributions have not been corrected for detection efficiency, but instead the Monte Carlo curves include the effects of detection efficiency. Whereas the $\cos\theta_\gamma$ distribution agrees reasonably well with both the spin 2 and spin 0 curves, the $\cos\theta_\eta$ distribution is fit much better by the spin 2 curve. This is primarily due to the excess of events with $|\cos\theta_\eta| > 0.9$. The insert in Fig. 27 shows these events on an expanded scale to show that there is no evidence of anomalous behavior due to these events (e.g., the events are spread out over the bin and do not cluster at $|\cos\theta_\eta| = 1.00$).

Table XI. Results of Angular Distribution Analysis for $\theta \to \eta\eta$

| Spin Hypothesis | Relative Probability |
|---|---|
| 2 | 1.0 |
| 0 | 0.045 |

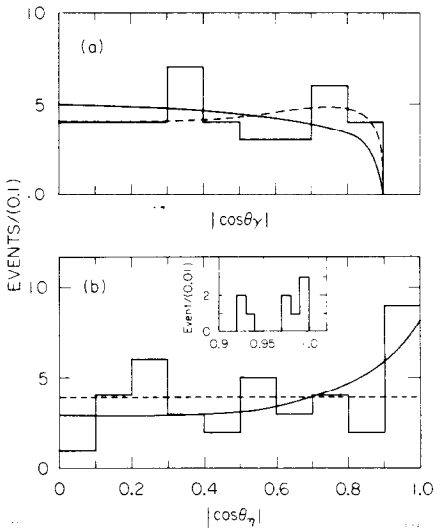


Fig. 27. a) $|\cos\theta_\gamma|$ and b) $|\cos\theta_\eta|$ distributions for $J/\psi \to \gamma\theta$, $\theta \to \eta\eta$. Solid curves are best fit distributions for spin 2. Dashed curves are expected distributions for spin 0. Insert shows events with $|\cos\theta_\eta| > 0.9$ with expanded scale. (Crystal Ball)

One runs into the standard problem when one attempts to understand the θ(1640) in terms of the ground state $J^{PC} = 2^{++}$ nonet. The f(1270) and f'(1515) are well-established members of this nonet. However, in this case, the mass of the θ is too low to consider the radial excitation hypothesis as a viable option.

The gluonium hypothesis is enticing as the θ has the quantum numbers of the 2-gluon ground state. However, the mass of the θ is in better agreement with the mass prediction for the $2^{++}$ excited state given in Table IX than the prediction for the ground state. On the other hand, it is likely that the spin splitting could push the $2^{++}$ ground state mass up high enough to agree with the experimental number. One calculation[39] of the $2^{++}$ ground state mass which takes into account the color magnetic interactions of gluons predicts a mass

of 1585 MeV. Another calculation[40] based on the interpretation of the $\iota(1440)$ as the $0^{-+}$ ground state predicts the lowest-lying $2^{++}$ state at a mass of 1650 MeV.

A less likely hypothesis is that the $\theta$ is a $q\bar{q}q\bar{q}$ state. A bag model calculation by Jaffe[41] predicts that the lowest-lying $2^{++}$ $q\bar{q}q\bar{q}$ state has a mass of 1650 MeV. Although the mass agreement is good, it is expected that if the $\theta$ were a $q\bar{q}q\bar{q}$ state, the width should be extremely large (much larger than the observed width) and there would be no evidence for resonant structure.[42]

C. $J/\psi \to \gamma f(1270)$

Although the process $J/\psi \to \gamma f(1270)$ may not be as exciting as the previous two radiative transitions, the analysis of this process provides a useful check on the analysis techniques employed in the $\iota$ and $\theta$ studies. It also provides a check that the Crystal Ball efficiencies are well understood. In addition, one hopes to find evidence for the $\theta$ or other new states in the process

$$J/\psi \to \gamma\pi^0\pi^0 \quad . \tag{6}$$

Figure 28 shows the $\pi^0\pi^0$ invariant mass distribution for events from the Crystal Ball which satisfy hypothesis (6).[43] The parameters of the f determined from a fit of this distribution to a Breit-Wigner plus a polynomial background ($M = 1260 \pm 15$ MeV and $\Gamma = 170 \pm 40$ MeV) agree with the standard values.[22] The branching ratio for $J/\psi \to \gamma f$ (corrected for all known decay modes) is $B(J/\psi \to \gamma f) = (1.48 \pm 0.25 \pm 0.30) \times 10^{-3}$. In order to extract an upper limit for the decay of the $\theta$ into $\pi^0\pi^0$, a fit which allowed Breit-Wigner contributions from both the f and the $\theta$ was made to the same distribution. The 90% confidence level upper limit is given in Table X.

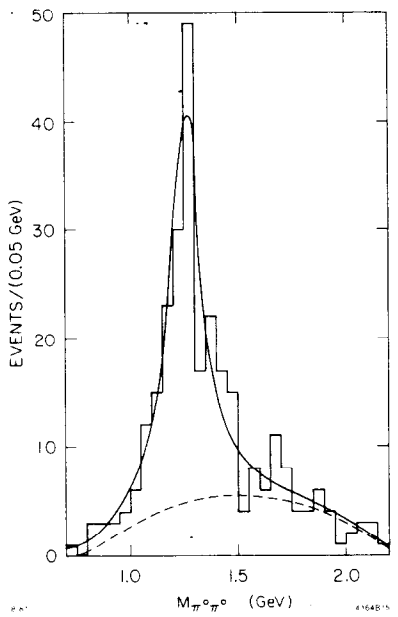


Fig. 28. $\pi^0\pi^0$ invariant mass distribution for events consistent with the hypothesis $J/\psi \to \gamma\pi^0\pi^0$. Solid curve represents fit to f(1270) plus background. Dashed curve represents background. (Crystal Ball)

Figure 29 shows the $\pi^+\pi^-$ invariant mass distribution for events from the Mark II[24] which satisfy constrained fits to the hypothesis

$$J/\psi \to \gamma\pi^+\pi^- \quad .$$

A background subtraction for feeddown from $J/\psi \to \rho\pi$ has been made. The remaining distribution is consistent with being almost entirely f(1270) as shown by the fitted curve. The branching ratio results for the Crystal Ball, Mark II, and previous experiments are summarized in Table XII.

Figure 30 shows the $\cos\theta_\gamma$ and $\cos\theta_{\pi^0}$ distributions from a spin analysis of the f(1270) data from the Crystal Ball. Spin 2 clearly provides a better fit to the data than

Table XII. $B(J/\psi \to \gamma f(1270))$

| Experiment | Decay Mode | $B(J/\psi \to \gamma f(1270))$ |
|---|---|---|
| Crystal Ball | $\pi^0\pi^0$ | $(1.48 \pm 0.25 \pm 0.30) \times 10^{-3}$ [a] |
| Mark II [b] | $\pi^+\pi^-$ | $(1.3 \pm 0.3) \times 10^{-3}$ |
| PLUTO [c] | $\pi^+\pi^-$ | $(2.0 \pm 0.3) \times 10^{-3}$ |
| DASP [d] | $\pi^+\pi^-$ | $(0.9 \pm 0.3) \times 10^{-3}$ or $(1.5 \pm 0.4) \times 10^{-3}$ [e] |

[a] First error is statistical; second is systematic.
[b] Ref. 24.
[c] Ref. 44.
[d] Ref. 45.
[e] Exact value depends on helicity of f in the final state.

spin 0. (The relative probability of the spin 0 hypothesis compared to the spin 2 hypothesis for the full 3-dimensional maximum likelihood fit is on the order of $10^{-11}$.) This gives one confidence in the reliability of the θ(1640) analysis.

Figure 31 shows a contour plot of y vs. x for f(1270) production. The data point and contours of equal probability are from the Crystal Ball analysis. The numbers associated with the contours give the number of standard deviations from the best value. (No systematic uncertainties are included in the errors.) Also shown are the theoretical predictions for pure M2 and E3 transitions (E1 is off scale), QCD,[47] and for tensor meson dominance.[48] The experimental measurement is inconsistent with all of these predictions. The helicity measurements from the Crystal Ball, Mark II (they have done a similar analysis), and PLUTO are given in Table XIII.

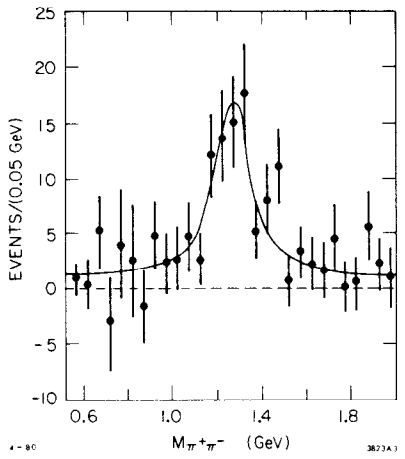


Fig. 29. $\pi^+\pi^-$ invariant mass distribution for events consistent with the hypothesis $J/\psi \to \gamma\pi^+\pi^-$. Curve represents fit to data. (Mark II)

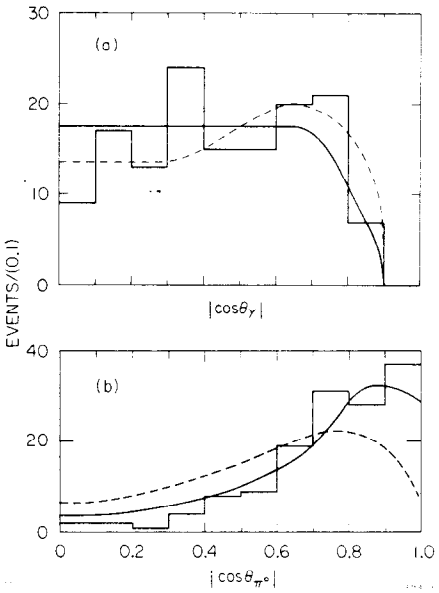


Fig. 30. a) $|\cos\theta_\gamma|$ and b) $|\cos\theta_{\pi^0}|$ distributions for $J/\psi \to \gamma f$, $f \to \pi^0\pi^0$. Solid curves are best fit distributions for spin 2. Dashed curves are expected distributions for spin 0. (Crystal Ball)

Table XIII. f(1270) Helicity Measurements

| Experiment | x | y |
|---|---|---|
| Crystal Ball | 0.88 ± 0.11 | 0.04 ± 0.14 |
| Mark II | 0.81 ± 0.16 | 0.02 ± 0.15 |
| PLUTO[a] | 0.6 ± 0.3 | $0.3\ ^{+0.6}_{-1.6}$ |

[a]Ref. 46.

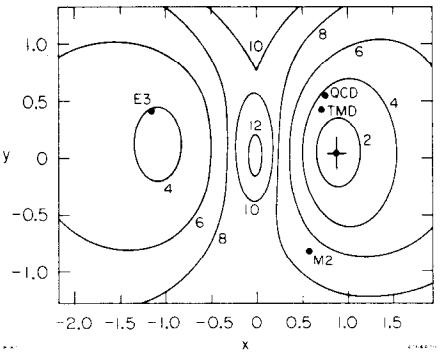


Fig. 31. Contour plot of y vs. x for f(1270) production. Data point and contours of equal probability are from Crystal Ball experiment. Theoretical points are referenced in text.

## IV. CONCLUSIONS

The Crystal Ball has evidence for an $\eta_c'$ candidate in the inclusive photon spectrum from the $\psi'$. The mass of the $\eta_c'$ candidate is M = 3592 ± 5 MeV.

A new state, the $\iota(1440)$, has been observed by both the Mark II and Crystal Ball collaborations in $J/\psi$ radiative decays. The spin-parity of the $\iota$ has been established to be $0^-$ by the Crystal Ball, and hence the $\iota(1440)$ is a different state than the E(1420). Possible interpretations of this state are as a gluonium resonance or as a radially excited state.

Another new state, the $\theta(1640)$, has been observed by the Crystal Ball in the decay $J/\psi \to \gamma\eta\eta$. The preferred spin for this state is 2. A possible interpretation of this state is as a gluonium resonance. Less likely is its interpretation as a $q\bar{q}q\bar{q}$ state.

## REFERENCES


1. D. Antreasyan, D. Aschman, E. Bloom, F. Bulos, T. Burnett, M. Cavalli-Sforza, R. Chestnut, D. Coyne, C. Edwards, J. Gaiser, D. Gelphman, G. Godfrey, Y. Gu, R. Hofstadter, R. Horisberger, M. Joy, C. Kiesling, I. Kirkbride, H. Kolanoski, W. Kollmann, K. Königsmann, W. Lavender, R. Lee, J. Leffler, A. Liberman, S. Lindgren, W. Lockman, S. Lowe, C. Newman, M. Oreglia, J. O'Reilly, A. Osterheld, R. Partridge, C. Peck, B. Pollock, F. Porter, M. Richardson, H. Sadrozinski, D. Scharre, K. Strauch, J. Tompkins, K. Wacker, A. Weinstein.

2. G. Abrams, M. Alam, C. Blocker, A. Blondel, A. Boyarski, M. Breidenbach, D. Burke, W. Carithers, W. Chinowsky, M. Coles, S. Cooper, W. Dieterle, J. Dillon, J. Dorenbosch, J. Dorfan, M. Eaton, G. Feldman, M. Franklin, G. Gidal, G. Goldhaber, G. Hanson, K. Hayes, T. Himel, D. Hitlin, R. Hollebeek, W. Innes, J. Jaros, P. Jenni, A. Johnson, J. Kadyk, A. Lankford, R. Larsen, M. Levi, V. Lüth, R. Millikan, M. Nelson, C. Pang, J. Patrick, M. Perl, B. Richter, A. Roussarie, D. Scharre, R. Schindler, R. Schwitters, J. Siegrist, J. Strait, H. Taureg, M. Tonutti, G. Trilling, E. Vella, R. Vidal, I. Videau, J. Weiss, H. Zaccone.

3. T. M. Himel et al., Phys. Rev. Lett. 44, 920 (1980).

4. M. Oreglia et al., Phys. Rev. Lett. 45, 959 (1980).

5. M. J. Oreglia, Stanford Linear Accelerator Center Report No. SLAC-236, Ph.D. Thesis, Stanford University, 1980 (unpublished).

6. F. Porter, Stanford Linear Accelerator Center Report No. SLAC-PUB-2785, to be published in the Proceedings of the 1981 EPS International Conference on High Energy Physics, Lisbon, Portugal, July 9-15, 1981.

7. E. D. Bloom, Stanford Linear Accelerator Center Report No. SLAC-PUB-2779, to be published in the Proceedings of the Sixteenth Rencontre de Moriond, Les Arcs, France, March 15-27, 1981.

8. D. L. Burke, Stanford Linear Accelerator Center Report No. SLAC-PUB-2745, to be published in the Proceedings of the Fourth International Colloquium on Photon-Photon Interactions, Paris, France, April 6-9, 1981.

9. J. Weiss et al., Phys. Lett. 101B, 439 (1981).

10. The Mark II detector is described in detail in R. Hollebeek, invited talk this conference.

11. R. Partridge et al., Phys. Rev. Lett. 45, 1150 (1980).

12. T. M. Himel et al., Phys. Rev. Lett. 45, 1146 (1980).

13. These inserts are based on a different spectrum than that shown in the main part of the figure. In addition, a background subtraction has been made.

14. The entire $\psi'$ data sample has been used in all analyses to be discussed from this point on.

15. The line shape is Gaussian except in the tails.

16. C. F. Biddick et al., Phys. Rev. Lett. 38, 1324 (1977).

17. E. Eichten, K. Gottfried, T. Kinoshita, K. D. Lane, and T. M. Yan, Phys. Rev. D 21, 203 (1980).

18. D. L. Scharre, Stanford Linear Accelerator Center Report No. SLAC-PUB-2761, to be published in the Proceedings of the International Conference on Physics in Collision: High Energy ee/ep/pp Interactions, Blacksburg, Va., May 28-31, 1981.

19. J. D. Bjorken, in Quantum Chromodynamics, edited by A. Mosher (Stanford, CA, 1980), p. 219; J. F. Donoghue, in Experimental Meson Spectroscopy - 1980, edited by S. U. Chung and S. J. Lindenbaum (AIP, New York, 1981), p. 104; J. F. Donoghue, in High Energy Physics - 1980, edited by L. Durand and L. G. Pondrom (AIP, New York, 1981), p. 35; P. M. Fishbane, to be published in the Proceedings of the 1981 Orbis Scientiae, Ft. Lauderdale, Fla., Jan. 19-23, 1981; and references therein.

20. T. Applequist, A. De Rújula, H. D. Politzer, and S. L. Glashow, Phys. Rev. Lett. 34, 365 (1975); S. J. Brodsky, T. A. DeGrand, R. R. Horgan, and D. G. Coyne, Phys. Lett. 73B, 203 (1978).

21. D. L. Scharre et al., Phys. Lett. 97B, 329 (1980).

22. Particle Data Group, Rev. Mod. Phys. 52, S1 (1980), and references therein.

23. Since only the angles but not the momenta of charged particles are measured by the Crystal Ball, only a 3-constraint (3C) fit is made to this process. (The $\pi^0$ mass is the third constraint.) In addition there is no particle identification for $K^{\pm}$. The kaon identification is by kinematics alone.

24. D. L. Scharre, in Experimental Meson Spectroscopy - 1980, edited by S. U. Chung and S. J. Lindenbaum (AIP, New York, 1981), p. 329.

25. K. Ishikawa, Phys. Rev. Lett. 46, 978 (1981); K. Ishikawa, Phys. Lett. 101B, 344 (1981); J. F. Donoghue, K. Johnson, B. A. Li, Phys. Lett. 99B, 416 (1981); M. Chanowitz, Phys. Rev. Lett. 46, 981 (1981).

26. C. E. Carlson, J. J. Coyne, P. M. Fishbane, F. Gross, and S. Meshkov, Phys. Lett. 98B, 110 (1981); H. J. Lipkin, Argonne National Laboratory Report No. ANL-HEP-PR-81-23 (1981); T. Barnes, Rutherford Laboratory Report No. RL-81-04 (1981).

27. C. Dionisi et al., Nucl. Phys. B169, 1 (1980).

28. P. Baillon et al., Nuovo Cimento 50A, 393 (1967).

29. See M. Chanowitz, ref. 25.

30. $J^P = 0^+$ is not allowed for a state decaying into three pseudoscalars. $J^P = 1^-$, although allowed for $K^*\bar{K}$ + c.c., would require the Dalitz plot to vanish at the boundaries, which is inconsistent with the data. Amplitudes with $J \geq 2$ were not considered.

31. D. J. Herndon, P. Soding, and R. J. Cashmore, Phys. Rev. D 11, 3165 (1975).

32. This would almost certainly not invalidate the results of the partial-wave analysis. Because the phase space in the $K\bar{K}$ system is so limited, the $K\bar{K}$ system is almost certainly in an S-wave, and hence, the spin-parity of the $K\bar{K}$ system is $0^+$.

33. This assumption is probably not a good one as the photon energy is large.

34. P. K. Kabir and A.J.G. Hey, Phys. Rev. D 13, 3161 (1976).

35. I. Cohen and H. J. Lipkin, Nucl. Phys. B151, 16 (1979).

36. N. P. Stanton et al., Phys. Rev. Lett. 42, 346 (1979).

37. R. L. Jaffe and K. Johnson, Phys. Lett. 60B, 201 (1976).

38. Although such a fit would ordinarily be a 4C fit, one constraint is removed in the determination of the vertex position along the beam direction which cannot otherwise be determined for an all neutral event.

39. K. Babu Joseph and M. N. Sreedharan Nair, Cohin University Preprint No. CUTP-81-1 (1981).

40. T. Barnes, Z. Phys. C 17, 679 (1981).

41. R. L. Jaffe, Phys. Rev. D 21, 281 (1977). See also B. A. Li and K. F. Liu, Stanford Linear Accelerator Center Report No. SLAC-PUB-2783, 1981 (submitted to Phys. Lett.).

42. R. Jaffe, invited talk this conference.

43. In nearly all events from this process, one or both $\pi^o$'s is sufficiently energetic that the two $\gamma$'s from the $\pi^o$ decay produce showers which overlap in the NaI and hence appear as a single neutral particle. However, these $\pi^o$'s can generally be differentiated from single $\gamma$'s by analysis of the shower pattern. In this final state, only events with four neutrals, one of which is identified as a $\pi^o$, are used.

44. G. Alexander et al., Phys. Lett. 72B, 493 (1978).

45. R. Brandelik et al., Phys. Lett. 74B, 292 (1978).

46. G. Alexander et al., Phys. Lett. 76B, 652 (1978).

47. M. Krammer, Phys. Lett. 74B, 361 (1978).

48. W. Gampp and H. Genz, Phys. Lett. 76B, 319 (1978).